Thin–Walled Structures 215 (2025) 113319

Contents lists available at ScienceDirect

Thin-Walled Structures

journal homepage: www.elsevier.com/locate/tws

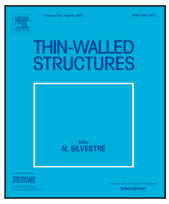

Full length article

Probabilistic analysis of cylindrical shells under continuously varying load combinations

Niklas Reuter *, Benedikt Kriegesmann

Hamburg University of Technology, Institute for Structural Mechanics in Lightweight Design, Hamburg, Germany

ARTICLE INFO

Keywords:
Buckling
Cylindrical shells
Combined loading

ABSTRACT

This paper presents a probabilistic design method for cylindrical shells under combined loading without explicitly simulating each load combination. Exemplarily, the combination of axial compression and torsion is considered. The probabilistically motivated design load is a quantile of the buckling load distribution. The stochastic distribution of the buckling load (and hence any quantile) differs for each combination of axial load and torsion. The basic idea of the presented method is to consider the buckling response as a random field, where the parameter describing the load ratio is the field variable. When this random field is characterized, the stochastic distribution may be determined for any load combination without explicitly running a probabilistic analysis for this load combination. This approach is compared to a more simple and straightforward approach of interpolating stochastic moments or quantiles between different load combinations.

1. Introduction

Thin-walled cylindrical shells are commonly used as structural elements in various fields, including aerospace and civil engineering. These shells are susceptible to buckling under specific types of loads, such as axial compression, torsion, bending, or hydrostatic pressure. The critical load at which buckling occurs, often referred to as the buckling load, is highly sensitive to a range of influencing factors [1]. The buckling behavior of cylindrical shells under axial compression and the various factors that can affect this behavior have been extensively studied over the past century. Several works have reviewed the theoretical and experimental developments in this area, including [2–5].

While it is common in practice for different critical buckling loads to occur in varying combinations, relatively little attention has been paid to the buckling of cylindrical shells under combined loading conditions. For instance, Winterstetter and Schmidt [6] conducted several experiments, primarily on metallic shells, where axial compression was combined with hydrostatic pressure, axial compression with torsional moments, or external pressure with torsion. Their results showed significant variability, with qualitatively different interaction curves between the buckling load and the various load combinations.

The design of cylindrical shell structures prone to buckling under various load combinations is addressed in established design guidelines such as NASA SP-8007 [1] and the European Standard EN 1993-1-6 (Eurocode 3) [7]. These guidelines were initially developed to provide lower-bound estimates for buckling loads in metallic cylinders, though NASA SP-8007 was later revised to include orthotropic materials and stiffened shells [1]. The interaction between different load types is treated differently in these two standards. NASA SP-8007 assumes a strictly linear interaction for any combination of simultaneous buckling-inducing loads [1], while Eurocode 3 allows for either linear or nonlinear interactions, depending on whether axial compression is combined with bending or torsion [7]. Both guidelines note that the assumptions underlying these interaction curves may lead to overly conservative designs and acknowledge the lack of experimental data needed to refine these approaches [1,7]. The authors recently published an experimental and numerical analysis of 22 cylindrical polymer cylinder under different combination of axial compression and bending [8]. Here, the change in buckling load distribution was small due to the small slenderness of the cylinders and the associated small sensitivity of geometric imperfections.

As a result of the realization that geometric imperfections significantly influence the buckling load of a circular cylindrical shell, Bolotin [9] proposed to analyze the buckling load probabilistically, since geometric imperfections are random in nature. Probabilistic methods allow to predict the scatter of the structural response (e.g. the buckling load) due to scattering input variables (e.g. material parameters, geometric imperfections, etc.) (see e.g. [10,11]). Bolotin [9] developed a first concept for the consideration of geometric imperfections, using a simplified imperfection model. Arbocz [12] showed that the characteristics of manufacturing-dependent geometric imperfections can be well described by Fourier series. Elishakoff and Arbocz

* Corresponding author.
E-mail address: niklas.reuter@tuhh.de (N. Reuter).

https://doi.org/10.1016/j.tws.2025.113319
Received 20 January 2025; Received in revised form 14 April 2025; Accepted 14 April 2025
Available online 22 May 2025

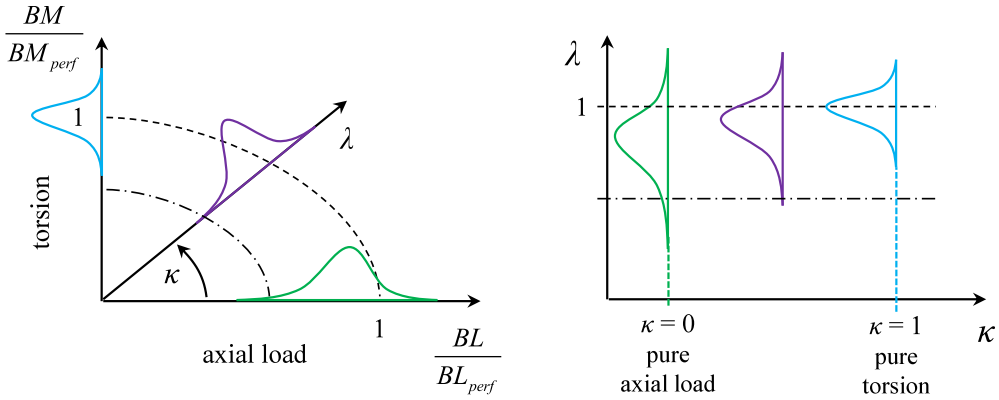

Fig. 1. Interaction diagram of axial load and torsional moment (left) and interpretation as a one-dimensional random field (right).

Fig. 2. First eigenmode under axial compression (left) and under torsion (right).

have probabilistically analyzed axially loaded circular cylindrical shells in various papers (see e.g. [13,14]), in which they parameterized the scatter of the imperfections with the Fourier coefficients. Papers dealing with probabilistic analysis or probabilistic design methods, especially of fiber composite cylinders, include those by Chryssanthopoulos et al. [15], Arbocz and Hilburger [16], Biagi and Del Medico [17], Chamis and Abumeri [18]. Since most of these works combined imperfection data from different circular cylinder shells, the predicted distribution could not be compared with an empirical distribution. A test series of ten nominally identical fiber composite cylinders at DLR in Braunschweig [19] allows the probabilistic prediction of the buckling load distribution to be compared [20,21].

To the best of the authors knowledge no approach has been published so far for a coherent probabilistic design approach for buckling prone structures under varying load combinations. The current paper exemplarily considers the combination of axial compression and torsion. As shown in Fig. 1, left, the stochastic distribution of the normalized buckling load factor λ generally changes with varying load combination. One obvious way to determine the stochastic distribution of the buckling load factor is to perform probabilistic analyses (e.g. Monte Carlo Analysis) for multiple load combinations. If the stochastic distribution of a load combination is of interest, which has not been analyzed, one might simply interpolate. This however raises the question for how many load combinations probabilistic analyses have to be performed in order to estimate the distribution of an interpolated load combination with a certain confidence.

Another way to look at this problem is to consider the bucking load factor λ as a random field as shown in Fig. 1, right. Consider the parameter κ as a normalized measure that describes the load ratio, which is chosen such that $\kappa = 0$ corresponds to pure axial compression and $\kappa = 1$ refers to pure torsion. As the load ratio may be chosen arbitrarily, κ is a continuous variable, and the stochastic distribution of λ varies gradually as κ changes. For similar values of κ, the distributions of λ is expected to be similar. The larger the difference of two κ the more pronounced the differences of the distributions. This relationship can be considered as a random field (or random process), in which κ is the field variable (or pseudo time of the process). Once this random field is characterized, the stochastic distribution of the buckling load can be determined for any load combination κ. The novel contribution of this paper is the aforementioned consideration of the buckling load factor as a random field and methods to characterize it. Furthermore, we suggest how to derive a probabilistically motivated design load as a function of κ.

The paper is structured as follows. First methods for determining buckling loads in particular under multiaxial loading are discussed. Then, approaches for determining the properties of the buckling load random field are presented. The proposed method is then demonstrated in the section numerical results.

2. Methodology

This section briefly recapitulates methods for determining buckling loads as well as the Monte Carlo method for probabilistic analyses. Then, a method for characterizing the random field of buckling load is presented in the last subsection.

2.1. Buckling analysis

Over the last century, numerous analytical and semi-analytical approaches have been developed that allow determining the buckling load of cylindrical shells. For an overview the interested reader is referred to [22]. Yet, the most flexible and recently mostly used method is the finite element method due to its generality. In the current contribution, we exclusively use finite element models for the buckling load prediction, where the type of analysis depends on whether a perfect or an imperfect cylinder is considered. For the nominal (perfect) geometry and material properties of cylinders, linear buckling analyses (LBA) are performed, by which eigenvalue and eigenmodes are determined (see, e.g., [23]). The first eigenvalue represents the first bifurcation point of the load–displacement curve. The buckling loads of the perfect shell under pure axial compression BL_{perf} and the buckling moment under pure torsion BM_{perf} are required for determining the normalized buckling load factor λ and the load combination factor κ, as described in the following subsection. The first eigenmodes of the cylinder considered in this paper under pure axial compression and under torsion are shown in Fig. 2.

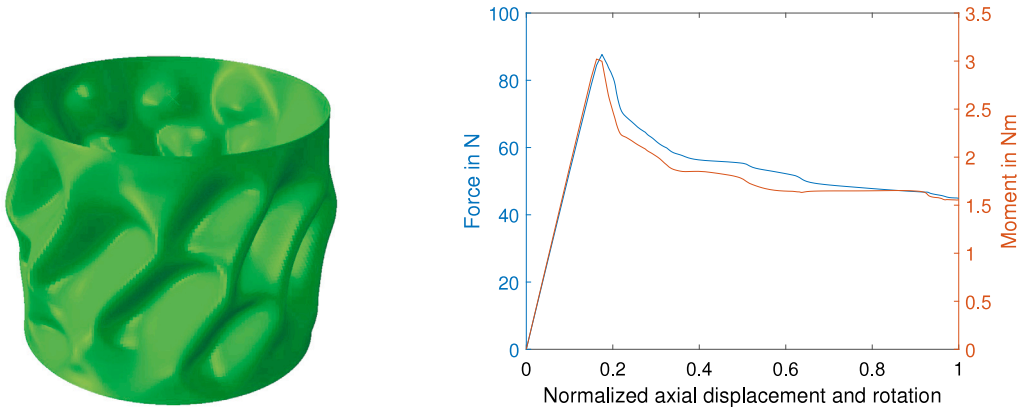

Fig. 3. Results of a displacement driven GNA with torsion and axial displacement: deformation with a scaling factor of 5 (left) and the load displacement curve of the simulation (right).

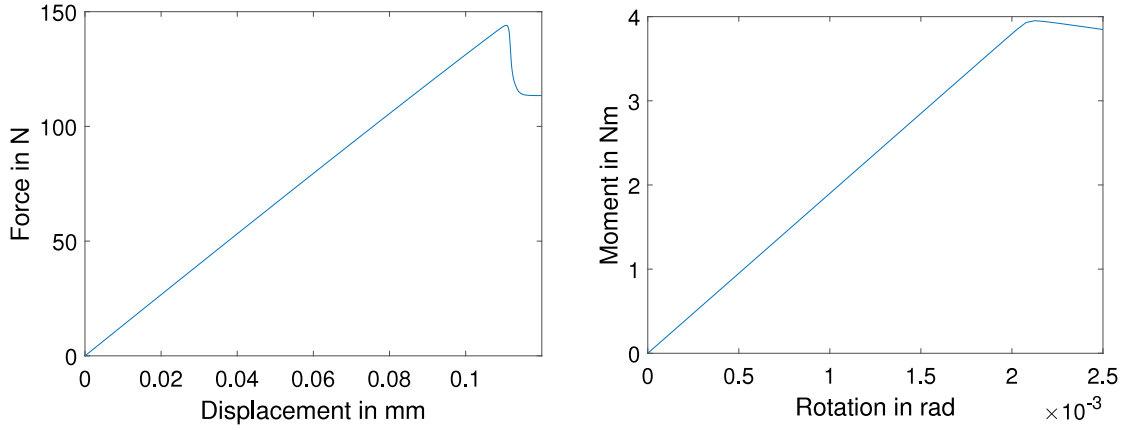

Fig. 4. Load–displacement curve for a displacement driven GNLA of an imperfect cylinder with pure axial displacement (left) and pure torsion (right).

For the analyses of imperfect cylinders with varying material properties and combined loading, geometrically nonlinear finite element analyses (GNLA) are carried out. These analyses must be run displacement driven, if the postbuckling behavior is of interest. Fig. 3 shows typical a postbuckling deformation, load–displacement curve and moment-displacement curve of the cylinder considered. For the probabilistic analyses presented in the remainder of the paper, only the highest buckling load and moment are desired. In this case, a load-driven analyses is used, which automatically aborts when the buckling load is reached.

2.2. Buckling under multiaxial loading

In the present paper, the cylindrical shells are loaded with both a torsion moment and axial compression simultaneously. In general it is possible that the maximal axial force and the maximal torsion moment do not occur simultaneously. In this case, the first drop of force or moment is considered as buckling. For the cylinders considered however, the drop of force and moment occurs simultaneously or almost simultaneously, as shown in Fig. 3, right. Fig. 4 shows the load–displacement curve for pure axial compression (left) and pure torsion (right). These show that under pure compression, the typical snap through buckling behavior is observed, that causes high imperfection sensitivity. Under pure torsion however, the load decreases very slowly after reaching its maximum, which indicates less imperfection sensitivity.

In order to be able to compare the distribution of the load carrying capability under different load combinations, the load factor λ is considered, which is defined as

$$\lambda = \sqrt{\left(\frac{BL}{BL_{perf}}\right)^2 + \left(\frac{BM}{BM_{perf}}\right)^2} \tag{1}$$

The load factor essentially describes the length of the vector which is spanned by the two normalized loads at which buckling occurs as visualized in Fig. 1, left. The buckling load BL_{perf} and buckling moment BM_{perf} which result from linear buckling analysis of the perfect shell are used for normalization.

In order to characterize the combination of axial compression and torsion, the parameter κ is introduced as follows.

$$\kappa = \frac{2}{\pi} \arctan\left(\frac{BM \cdot BL_{perf}}{BM_{perf} \cdot BL}\right) \tag{2}$$

The parameter κ is linked to the angle of the load vector in the normalized space of axial load and torsion (see Fig. 1, left). It is normalized such that $\kappa = 0$ refers to pure axial compression and $\kappa = 1$ refers to pure torsion.[1]

2.3. Monte Carlo analysis

For the estimation of the stochastic distribution of buckling loads, we use Monte Carlo simulations in this paper. The Monte Carlo method

[1] In these extreme cases of $\kappa = 0$ and $\kappa = 1$, eq. is not defined, as there is no buckling moment in pure axial compression and no buckling load in pure torsion. Hence, the terms BM and BM_{perf} are neglected for $\kappa = 0$ and BL and BL_{perf} are neglected for $\kappa = 1$.

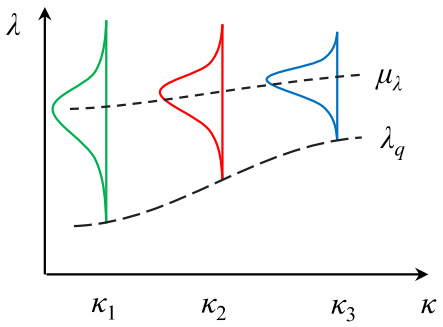

Fig. 5. Example of different distributions of the buckling load factor λ as a function of the load ratio κ.

is the most flexible, despite numerically most costly method for uncertainty quantification. More efficient method either use Taylor expansion approximations of the buckling load (such as first-order second-moment methods), importance sampling or training of surrogate models with a subset of the realizations. The focus of this paper however is not the uncertainty quantification method itself. In order to exclude effects that might originate from the method used for uncertainty quantification, the plain Monte Carlo method is used. The basic idea is to generate a large number of realizations of stochastic input parameters and evaluate the objective function (here the buckling load) for each realization. The stochastic distribution of the input parameters is derived from measurements. The Monte Carlo simulation results in a discrete distribution of the objective function, from which stochastic moments (such as mean value and variance) as well as quantiles (for instance, the buckling load that is exceeded with a probability of 99%) can be derived.

2.4. Interpolation of stochastic moments and quantiles

The following section considers the situation that the stochastic distribution of buckling load has been determined for certain load combinations κ_i, as shown in Fig. 5 for the example of three load combinations. Now consider that a stochastic moment like the mean μ_λ or a quantile λ_q is of interest for a load combination κ that has not been analyzed so far. One obvious option is to perform a probabilistic analysis for the desired load combination, which is also the most expensive solution. Another option is to interpolate the quantity of interest, which we discuss in the following Section 2.4.1. A further alternative is to approximate the covariance function of the random field of buckling load, which is discussed in Section 2.4.2.

2.4.1. Interpolation of moments and quantiles

In general, any regression method (or surrogate model) may be used for the interpolation of the quantities of interest. We decided to use the well-established Kriging approach (see, e.g., [24]) for the following reasons. Firstly, Kriging is known to perform well even for a small amount of data. Secondly, Kriging provides the exact value for input values that are used to set up the surrogate model. And finally, Kriging provides a measure for the prediction accuracy over the domain considered. In the context of cylinder buckling, Kriging has been used for instance by Wang et al. [25] to account for manufacturing uncertainties in the filament winding. The authors are however not aware of any reference where it has been used to interpolate the buckling load for different load cases.

Given that the stochastic distribution of buckling load has already been determined (e.g. by Monte Carlo analyses) for discrete load combinations κ_i, Kriging can be used to interpolate a quantity of interest for any other load combination κ. For instance, if the quantity of interest is the quantile λ_q, its Kriging estimator $\hat{\lambda}_q$ for any κ is given by

$$\lambda_q(\kappa) \approx \hat{\lambda}_q(\kappa) = \boldsymbol{f}(\kappa)^T \boldsymbol{\beta} + \boldsymbol{r}(\kappa)^T \boldsymbol{R}^{-1}(\boldsymbol{\Lambda}_q - \boldsymbol{F}\,\boldsymbol{\beta}) \tag{3}$$

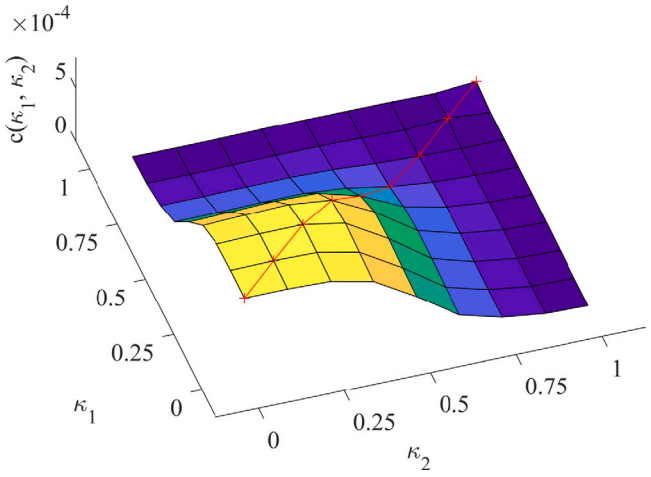

Fig. 6. Example of a two-dimensional non-stationary (auto)covariance function, where the function of the variance (red line) is on the bisector.

Here, $\mathbf{F}$ is the Vandermonde matrix of the assumed polynomial, $\mathbf{R}$ is the correlation matrix of training data, $\boldsymbol{\beta}$ is a vector with polynomial regression parameters, $\boldsymbol{r}$ is a vector with correlations of κ to training data, and $\boldsymbol{\Lambda}_q$ contains the output training data. The obtained interpolation qualitatively looks like the dashed line in Fig. 5. The same approach can be applied to the mean value, the variance, or any other measure that can be obtained from the distribution at the discrete points.

2.4.2. Approximation of the covariance function

If the probabilistic analyses depicted in Fig. 5 are carried out with the same set of realizations of input parameters, it is easy to determine the correlation (i.e. the covariance) of different load cases. This information has not been used in the previous subsection. In this subsection it is described how the covariances can be used to interpolate the variance.

Random fields can be characterized by their trend (function of the mean value) and their covariance function. The random field of the load factor λ is non-stationary.[2] Given the situation shown in Fig. 5, the mean can be estimated from all load cases analyses and then interpolated as described in the previous section. Estimating the covariance function is less straightforward.

In general, for a one-dimensional random field with field variable κ the (auto)covariance function is a two-dimensional function $c(\kappa_1, \kappa_2)$. Fig. 6 shows an example of a non-stationary covariance function. Due to the non-stationarity, c cannot be approximated with well-known correlation functions, that are only function of the distance $|\kappa_1 - \kappa_2|$. However, if from multiple Monte Carlo analyses the variance and covariance for multiple combinations of different κ_i are known, the two-dimensional function of c can be approximated by interpolation, for instance using Kriging. Now, the Kriging estimator reads

$$c(\kappa_1, \kappa_2) \approx \hat{c}(\kappa_1, \kappa_2) = \boldsymbol{f}(\kappa_1, \kappa_2)^T \boldsymbol{\beta} + \boldsymbol{r}(\kappa_1, \kappa_2)^T \boldsymbol{R}^{-1}(\boldsymbol{C} - \boldsymbol{F}\,\boldsymbol{\beta}) \tag{4}$$

Here, $\boldsymbol{C}$ is a vector with covariances at the already evaluated combinations of κ.

Once a Kriging model is set up, the variance σ_λ^2 can be approximated by

$$\sigma_\lambda^2(\kappa) \approx \hat{c}(\kappa, \kappa) \tag{5}$$

In other words, the Kriging model, which represents the whole surface in Fig. 6, is used to interpolate along the red line in Fig. 6. The possible advantage over the method described in the previous subsection lies in the fact that now also the information about the covariances are used.

[2] In case the load factor turns out to be stationary, no interpolation is required as stochastic moments and quantiles are constant.

Fig. 7. One of the polymer cylinders from [8], of which the imperfections are used to generate random samples.

Table 1
Geometry and material data of the cylinder.

Length	Radius	Thickness	Young's Modulus	Poisson's ratio
100 mm	60 mm	0.2 mm	1800 MPa	0.3

3. Numerical results

The methods presented in the previous section are applied to a polymer cylinder, for which the measured geometric imperfections are provided in [8]. These cylinders have been tested in axial compression with varying eccentricity, causing a bending moment. The methods presented before could be applied to a combination of axial compression and bending. However, the tests and simulations in [8] revealed that the stochastic distribution does not change significantly when varying the combination of axial load and bending. This is different for the combination of axial load and torsion, as presented in this section. Therefore, the combination of torsion and axial load is considered in the following, even though no test results are available for this load combination.

3.1. Cylinder model

The cylinders considered here are shown in Fig. 7 as reference. The parts for clamping of the cylinders are not considered in the simulation, but only the free length. The nominal cylinder geometry and material properties are listed in Table 1. The cylinders from [8] have a relatively low radius to thickness ratio (R/t) because of the relatively high nominal thickness of 1 mm. With a nominal radius of 60 mm, the R/t results in 60. Since cylinders of this slenderness are known to have a small imperfection sensitivity, the thickness is assumed to equal 0.2 mm, which results in a $R/t = 300$. The imperfections are assumed to be the same as for the original cylinders and therefore, the w/t ratio scales by factor 5. In the work of [8], the Young's modulus of the cylinders of approximately 1800 MPa is specified. The Poisons ratio of $\nu = 0.3$ is chosen.

The finite element model of the cylinder is set up in Abaqus using linear shell elements with reduced integration (S4R). The finite element mesh consists of 360 elements in circumferential and 100 elements in axial direction.

In order to be able to investigate the buckling loads from geometric non-linear analysis, the measured geometry of 22 cylinders from [8] are used. The work provides Fourier Coefficients (FC) of the measured geometric imperfections. From the provided FC the imperfection $\overline{W}$ of the cylinder can be calculated using Eq. (6). The bounds of the sums are $n_1 = 39$ and $n_2 = 19$, which results in $40 \cdot 20 = 800$ FC in total per cylinder.

$$\overline{W}(x,y) = 2t \sum_{k=0}^{n_1} \sum_{l=0}^{n_2} cos\frac{k\pi x}{L}\left(A_{kl} cos\frac{ly}{R} + B_{kl} sin\frac{ly}{R}\right) \tag{6}$$

It is assumed, that the geometric imperfections are not affected by a lower thickness since they only measure the deviation from the initial radius in radial direction. Therefore, the FC remain the same. For the Monte Carlo analysis 200 random realization of geometric imperfections are generated. The random Fourier coefficients are generated in the same way as in [8]. The FC are assembled in the random vector $\mathbf{Y}$, which has the covariance matrix $\mathbf{\Sigma_Y}$ and the mean vector $\boldsymbol{\mu_Y}$. Kolmogorov-Smirnoff tests (KS test) of the FCs show that they can be modeled as Gauss distributed. A random vector $\mathbf{z}$ with uncorrelated entries and standard Gauss distribution (i.e. zero mean and variance of one) can easily be generate. Using Eq. (7) a realization of $\mathbf{z}$ is transformed to a realization of $\mathbf{y}$.

$$\mathbf{y} = \mathbf{\Sigma}_{\mathbf{y}}^{\frac{1}{2}}\mathbf{z} + \boldsymbol{\mu}_{\boldsymbol{y}} \tag{7}$$

As KS tests can also be used to compare two discrete distributions, KS tests were used to check if the generated FC follow the same distributions as the input FCs (e.g. the FC from measurements). With a significance level of 1 %, all of the FCs passed this check. The imperfection amplitude to thickness ratio (w/t) ranges from $2 \cdot 10^{-6}$ to 3.595. The mean values of w/t over one random sample ranges from 0.297 to 2.133.

In addition to that, the material properties (Young's modulus and Poisson's ratio) and the thickness of 0.2 mm are considered constant. For clamping, a fixed clamping of the bottom nodes is considered. The load is introduced by a node in the center of the nodes at the top of the cylinders, which are connected with a fixed rigid body constraint of the top nodes. These nodes are free in rotation and free in axial direction. The load case of pure compression is achieved by a force in the axial direction of the cylinder and for pure torsion a moment around the cylinder axis is introduces. For a combined loading, both loads are introduced simultaneously with a constant predefined ratio.

3.2. Deterministic buckling analysis

For determining the normalized load factors according to Eq. (1), the buckling load for pure axial compression and pure torsion of a perfect cylinder without imperfections are calculated using the LBA. These analyses provide a buckling load of 276.68 N and a buckling torsion moment of 4.13 Nm. The associated buckling modes are shown in Fig. 2.

Fig. 3 shows the deformed cylinder and the load–displacement plot of a displacement driven GNLA with a random geometric imperfection, with a total rotation around the cylinder axis of 0.01° and total axial displacement of 0.4 mm. The load–displacement plot includes two ordinates, one for the axial force and the one for the torsion moment. The abscissa is normalized to the maximal deformation, i.e. axial displacement for the force and rotation for the torsion. The displacement driven analysis allows to capture the postbuckling behavior of the cylinder. The plot shows, that when buckling occurs, the axial load and the torsion moment drop simultaneously. The maximum loads (axial compression and torsion) will be called buckling loads in the following. The post buckling behavior yields a non-linear course with several more kinks. These kinks can be explained with the changing of the buckling pattern.

3.3. Monte Carlo simulation of the buckling load

For the Monte Carlo analyses, different load cases are considered. Pure axial compression ($\kappa = 0$), pure torsion ($\kappa = 1$) and seven different combinations, varying κ in steps of $\Delta\kappa = 0.125$ are considered. 200

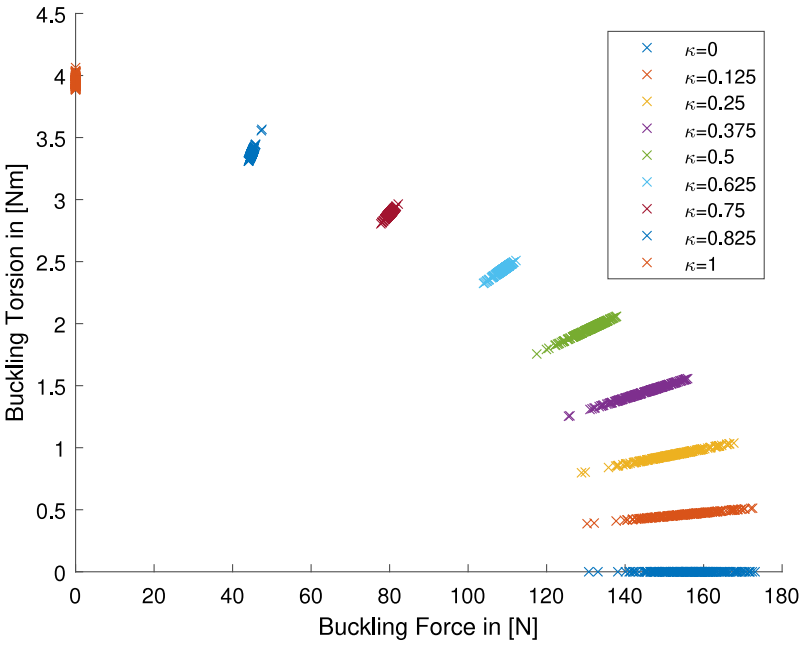

Fig. 8. Buckling loads and moments originating from Monte Carlo simulations with different load combinations κ.

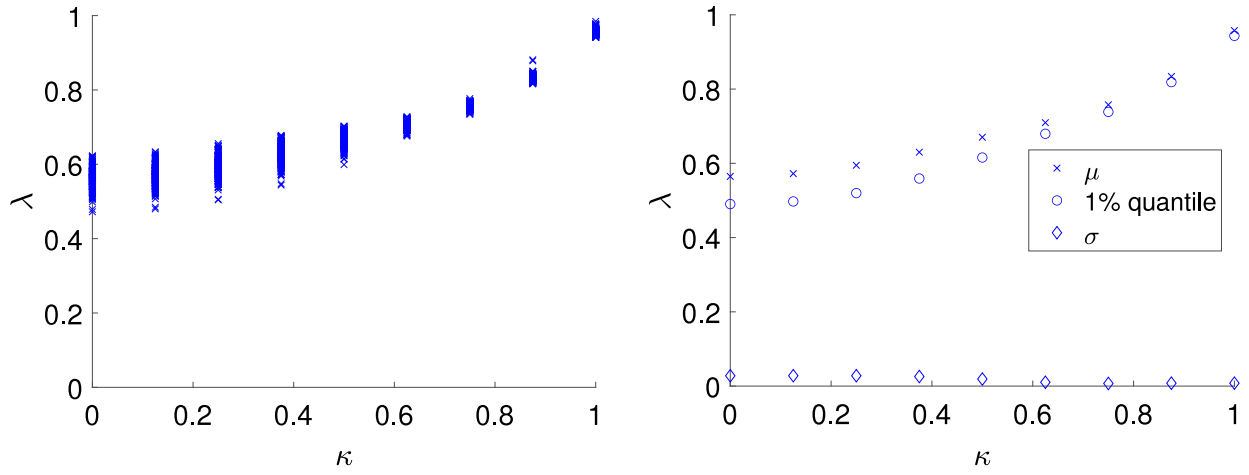

Fig. 9. Normalized buckling load factor λ from Monte Carlo simulations with 200 samples for different load combination κ (left) and the resulting mean value, standard deviation and 1% quantile of the load factor for different load combination (right).

realizations of random input parameters are generated. Each realization is analyzed for each of the nine load cases. For each realization and load case, a load-driven GNLA is performed to determine the buckling load. Fig. 8 shows the buckling loads and moments for every simulation conducted within the Monte Carlo simulations. The two outliers which occur for $\kappa = 0$ to $\kappa = 0.375$ refer to the same two realizations. The imperfection patterns of these cylinders seem to influence the buckling loads with a high ratio of axial compression strongly, although their imperfections do not differ visibly (i.e. similar w/t ratio as other realizations).

For Fig. 9 (left) the results from Fig. 8 are normalized according to Eq. (1) and plotted over the load combination parameter κ. This visualization is the discrete version of Fig. 1, right. The set of buckling loads obtained with one random realization for different load combinations κ can be regarded as one realization of the random field of λ. In Fig. 9 (right), the mean value, standard deviation and 1% quantile of the buckling load factor, which are determined from the Monte Carlo simulations, are plotter over κ, which indicates the nonstationarity of the random field. The 1% quantile can be considered as a probabilistically motivated design load. It corresponds to the so called A-basis design allowable (“A-value”).

Fig. 10 shows the histograms of λ for the load case of pure axial compression and pure torsion respectively. Table 2 summarized the mean values and standard deviations of the axial buckling load, the buckling torsion moment and the normalized load factor λ. For λ, the 1% quantile is also included in the table, which can be interpreted as a probabilistically motivated design load. The standard deviation of λ decreases drastically for higher values of κ while the mean value increases. Comparing pure axial compression and pure torsion shows a high discrepancy in both mean value and standard deviation. In addition to the mean value and the 1% quantile of λ, the skewness over every κ was evaluated. The skewness changes drastically from negative values to positive values, which indicates that the distribution type changes for different κ. Therefore, the distribution type of λ for every κ was checked with Kolmogorov-Smirnoff tests (KS tests). In a KS test, the largest difference d of two cumulative distribution functions (cdf) is determined to decide where a discrete distribution follows some assumed distribution type (see, e.g., [10]). Table 3 shows the d-values

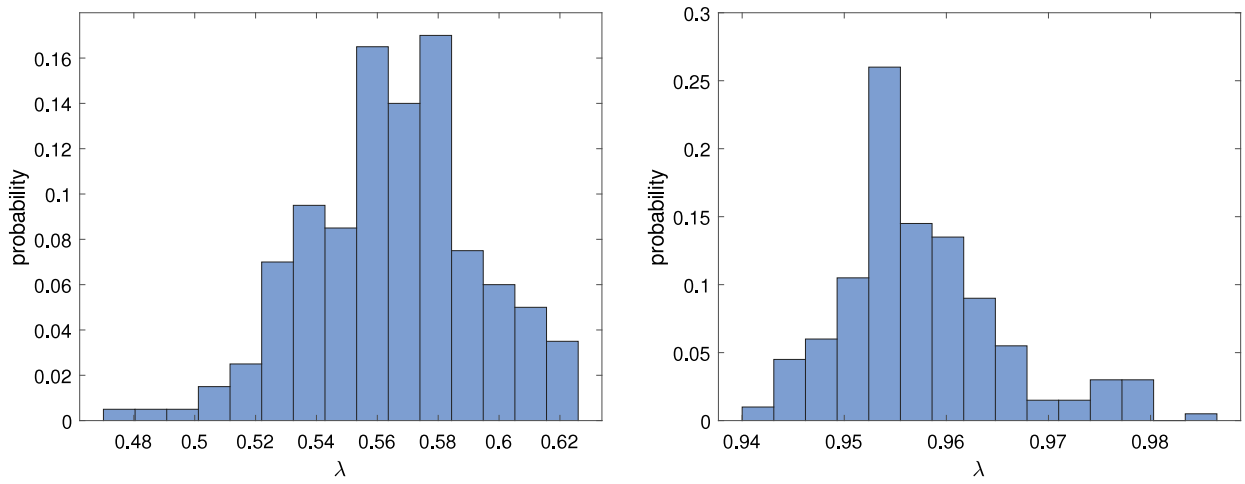

Fig. 10. Histograms of the buckling load factor λ for pure axial compression (left) and pure torsion (right) resulting from Monte Carlo simulations.

Table 2
Mean values μ and standard deviations σ of the buckling loads BL and buckling moments BM and normalized buckling load λ determined with Monte Carlo analyses.

κ	0	0.125	0.25	0.375	0.5	0.625	0.75	0.875	1
μ_{BL} in N	156.22	155.25	151.94	144.80	130.96	108.86	80.06	44.89	0.00
σ_{BL} in N	7.70	7.58	7.13	5.93	3.71	1.57	0.74	0.42	0.00
μ_{BM} in Nm	0.00	0.46	0.94	1.44	1.96	2.43	2.89	3.37	3.95
σ_{BM} in Nm	0.00	0.02	0.04	0.06	0.06	0.04	0.03	0.03	0.03
μ_λ	0.5647	0.5723	0.5947	0.6300	0.6703	0.7095	0.7576	0.8339	0.9576
σ_λ	0.0278	0.0280	0.0279	0.0258	0.0190	0.0103	0.0070	0.0078	0.0079
1% quantile of λ	0.4902	0.4973	0.5198	0.5591	0.6156	0.6796	0.7386	0.8187	0.9433
Skewness of λ	−0.2532	−0.2393	−0.2655	−0.4177	−0.6866	−0.7183	−0.3066	2.0927	0.9030

Table 3
d-values of KS tests for every κ with different distribution types, where the minimal and therefore best-matching values are bold.

κ	Tested distribution				
	Gauss	Beta	Gamma	Laplace	Gumbel
0	**0.0375**	0.0615	0.0426	0.0821	0.1024
0.125	**0.0422**	0.0568	0.0479	0.0959	0.1085
0.25	**0.0363**	0.0576	0.0424	0.0918	0.1066
0.375	0.0590	**0.0479**	0.0641	0.1088	0.1277
0.5	0.0674	**0.0408**	0.0711	0.1234	0.1378
0.625	0.0598	**0.0591**	0.0613	0.1138	0.1214
0.75	0.0556	0.0717	**0.0556**	0.1084	0.1010
0.875	0.1104	0.1078	0.1095	**0.0700**	0.1003
1	0.1102	0.1239	0.1091	0.1445	**0.0994**

of the KS tests for different values of κ and five chosen distribution types. For each load combination κ, the best (smallest) d-value is printed bold. The results shown that the random field of $\lambda(\kappa)$ is indeed non-stationary.

3.4. Interpolation of arbitrary load combinations with Kriging

The mean values, standard deviations and 1% quantiles obtained by MC analyses are shown in Fig. 9 (right) for 9 different load combinations. Figs. 11–13 show the same results together with a Kriging interpolation of these values, as described in Section 2.4.1. Thereby, the probabilistic quantities are obtained for arbitrary values of κ without performing additional MC analysis of the desired load combination. For the Kriging interpolation a Gaussian correlation model, and a first-order polynomial regression model is used. The variance is interpolated with both methods, the direct interpolation of the variance values and the interpolation of the covariance function as described in Section 2.4.2. Both approaches provide almost the same interpolated values, except an oscillation of the covariance Kriging for $0.875 < \kappa < 1$.

3.5. Comparison with deterministic approaches

The NASA SP-8007 design guideline [1] for the design loads of cylinders under axial compression and torsion is applied for the investigated cylinders. The knockdown factor γ (KDF) for axial compression is calculated with Eq. (8) which results in $\gamma = 0.4042$. For torsion, Eq. (9) and Eq. (10) are applied which results in a critical torsion moment of $T_{cr} = 2.529$ Nm and a KDF for torsion of 0.6122. For combined loading, the guideline suggests a linear interpolation of the normalized design load factors. This allows a comparison with the present approach, which is shown in Fig. 14. The design load given by the NASA SP-8007 is lower than the 1% quantile for every load combination for the cylinders considered. Moreover, the qualitative evolutions of the design loads over the load ratio κ differ significantly, indicating different levels of conservatism of the KDF-based approach.

$$\gamma = 1 - 0.901\left(1 - e^{-\frac{1}{16}\sqrt{\frac{R}{t}}}\right) \tag{8}$$

$$T_{cr} = \frac{\pi\left(R_o^4 - R_i^4\right)\tau_{cr}}{2R} \tag{9}$$

$$\tau_{cr} = \frac{0.5005 \cdot E}{\left(\frac{R}{t}\right)^{\frac{5}{4}}\left(\frac{L}{R}\right)^{\frac{1}{2}}} \tag{10}$$

In addition to this design guideline, the Single Perturbation Load Approach (SPLA) introduced by Hühne et al. [26] is applied. Its basic idea is to apply a perturbation load in radial direction at half cylinder height, and then determine the buckling load. This is repeated for increasing perturbation loads, which typically provides a diagram as shown for pure compression in Fig. 15 (blue crosses). The load level at which the buckling load starts to decrease slower is considered as design load. Though this approach was developed for axially compressed cylinders, the behavior under combined loading is investigated here.

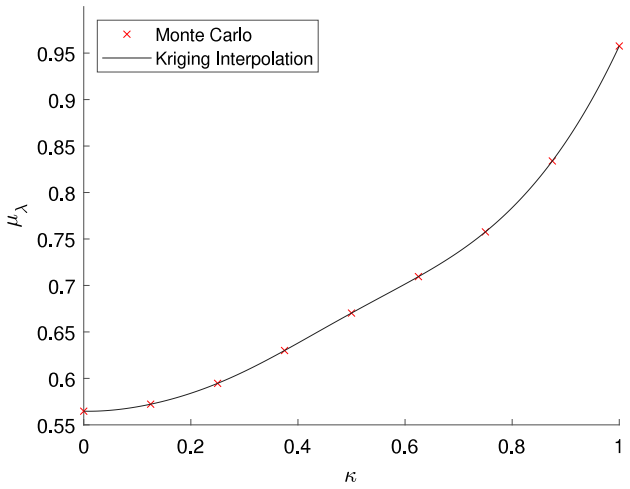

Fig. 11. Mean value λ with experiment data and interpolation with Kriging using all calculated load cases.

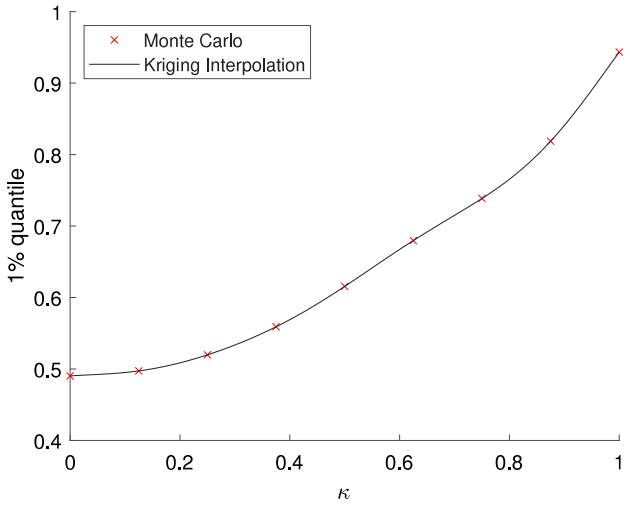

Fig. 12. 1% quantile of λ with experiment data and interpolation with Kriging using all calculated load cases.

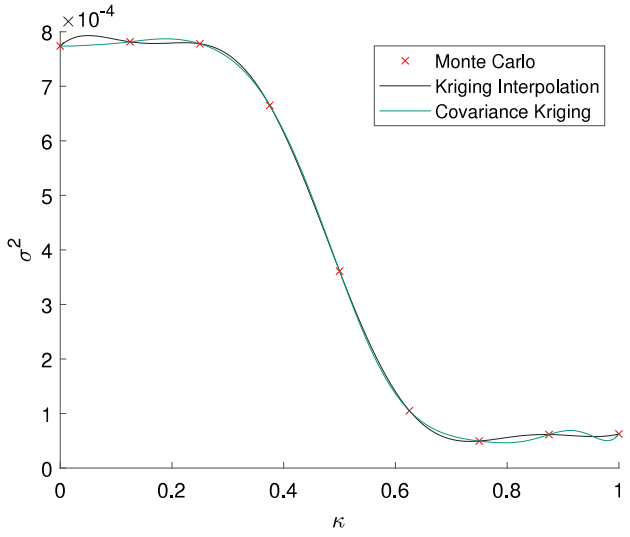

Fig. 13. Variance of λ with experiment data and interpolation with Kriging and Covariance Kriging using all calculated load cases.

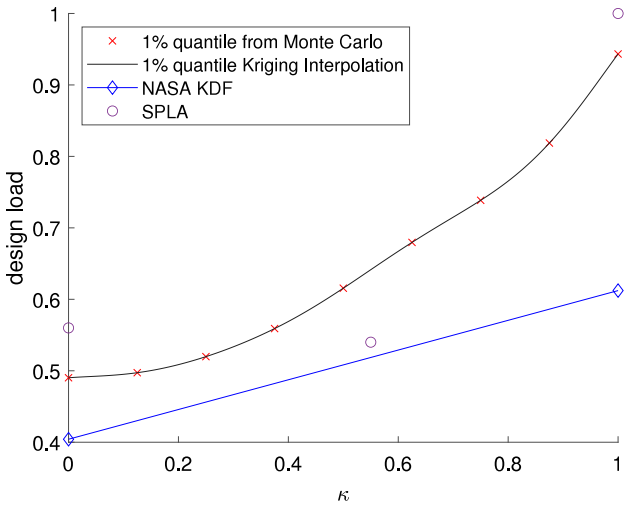

Fig. 14. NASA SP-8007 and SPLA design loads compared to 1% quantile obtained form Monte Carlo simulations for the investigated cylinders.

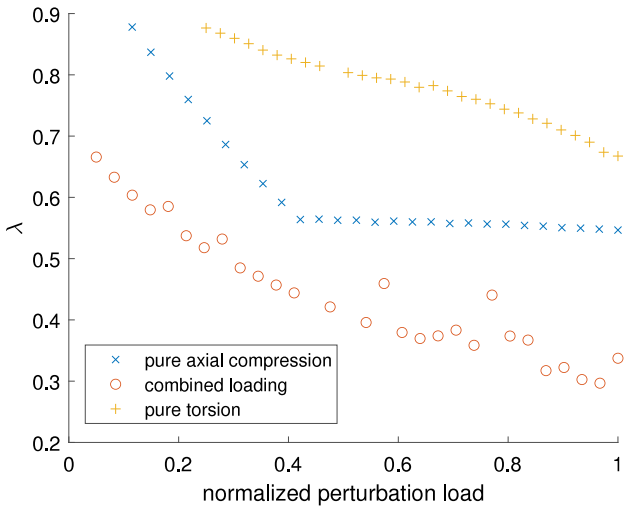

Fig. 15. Normalized results of the Single Perturbation Load approach applied to the cylinder considered for different load combinations.

For better comparability, the results in Fig. 15 are normalized. The buckling load factor λ is determined as before and the perturbation loads are divided by the largest perturbation load that is applied. This maximal perturbation load equals 0.15N for pure axial compression, 4N for combined loading and 6N for pure torsion.

For pure compression, the SPLA provides a design load of approximately $156N$. For pure torsion, the typical behavior cannot be observed and the perturbation loads need to be much higher in order to influence the buckling moment. The SPLA is also applied to a combination of torsion and axial compression. Since the FE analysis has to be displacement driven, the ratio of axial compression and torsion cannot be set precisely and scatter around $\kappa = 0.55$. The design load cannot be identified clearly, but is chosen to $\lambda \approx 0.54$ (intersection of upper outliers and lower bound).

The results indicate that the SPLA cannot be applied to pure torsion. This is not surprising, as the torsional buckling moment is less sensitive to geometric imperfections than the axial buckling load and the SPLA is known to mainly cover geometric imperfection sensitivity [27]. Consequently, for combined loading the SPLA becomes less conservative the smaller the contribution of axial loading (here as κ approaches 1).

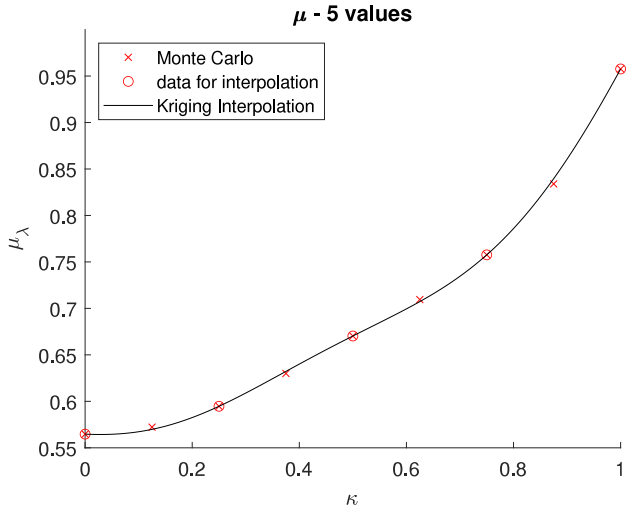

Fig. 16. Mean value of λ with experiment data and interpolation with Kriging with 5 load cases.

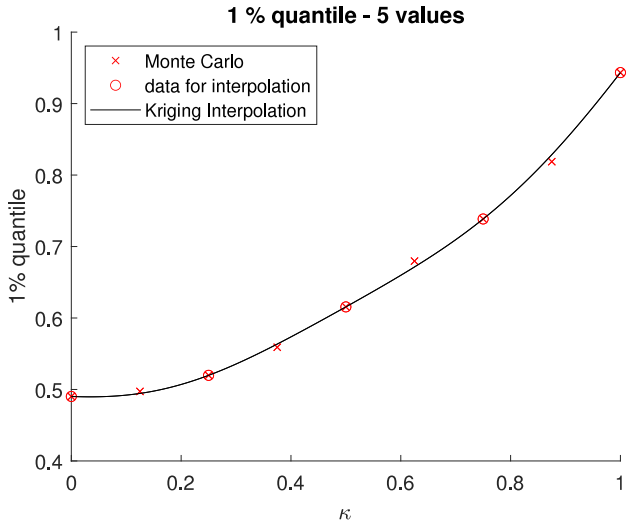

Fig. 17. 1% quantile of λ with experiment data and interpolation with Kriging with 5 load cases.

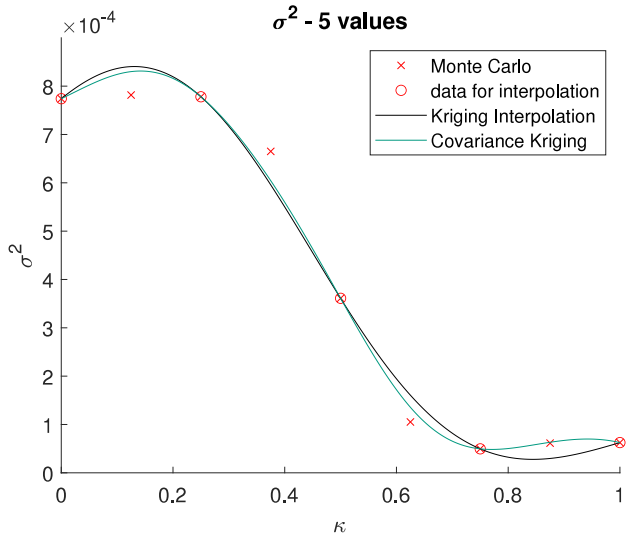

Fig. 18. Variance of λ with experiment data and interpolation with Kriging and Covariance Kriging using 5 load cases.

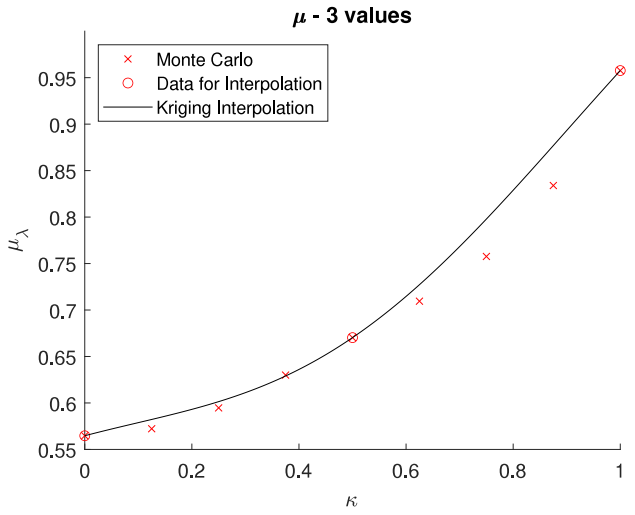

Fig. 19. Mean value of λ with experiment data and interpolation with Kriging with 3 load cases.

3.6. Interpolation with a reduced number of considered load cases

In this section it is assumed, that not for all 9 load cases a MCA was performed. The interpolation is therefore performed for only a reduced number of load cases but will be compared to the actual results. The comparison shows how accurate the not included load cases are predicted. The idea is to investigate how many MCA of different combinations are required for a good approximation. Since this is of course case-dependent we additionally demonstrate how it can be accessed if enough load cases have been analyzed. Figs. 16–18 show the interpolation with 5 load cases (evenly from $\kappa = 0$ to $\kappa = 1$) and Figs. 19–21 show the result if only three load cases ($\kappa = 0$, $\kappa = 0.5$, $\kappa = 1$) are taken into account. For the interpolation of the variance, the two approaches are depicted in the Figures. The direct interpolation of the variance and the interpolation of the variance using the covariance matrix yield in good approximations of the variance. Using alternative kernels for the correlation functions such as Matérn did not improve the results.

The Table 4 shows the relative mean error for the different interpolations at the points which were excluded for the interpolation. The

Table 4
Mean of the relative error at the interpolated κ values.

	5 load cases	3 load cases
μ	0.48%	1.94%
1% quantile	0.99%	1.47%
σ^2 Kriging Interpolation	11.75%	93.00%
σ^2 Covariance Kriging	30.56%	109.86%

interpolation of μ and the 1% quantile yield very good approximations also for a reduced number of load cases. The biggest discrepancy can be found in the interpolation of σ^2 with only 3 load cases. The reason for that is the change of the data in the range where no data is used for the interpolation.

The reduction of the number of load cases reduces the computational cost. With a number of desired load cases $n = 9$ in the present case, every interpolated case reduces the computational time by $\frac{1}{n}$ under the assumption that the computational time for every realization is constant and the computational time for the interpolation is negligible. The reduction to 5 load cases therefore reduces the computational time to 56 % of the initial computational time and the reduction to 3 load

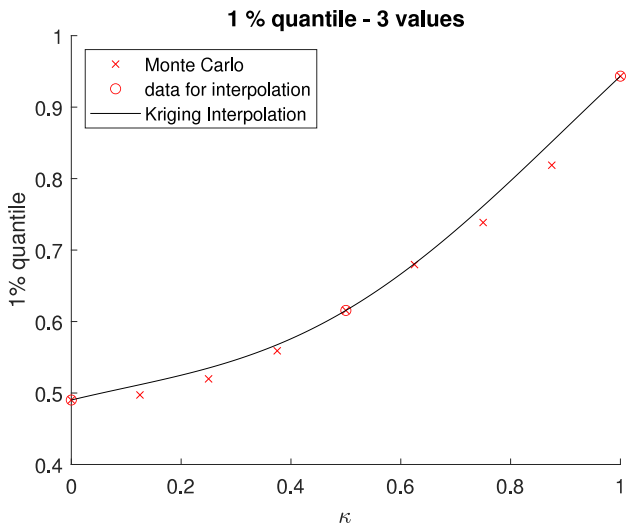

Fig. 20. 1% quantile of λ with experiment data and interpolation with Kriging with 3 load cases.

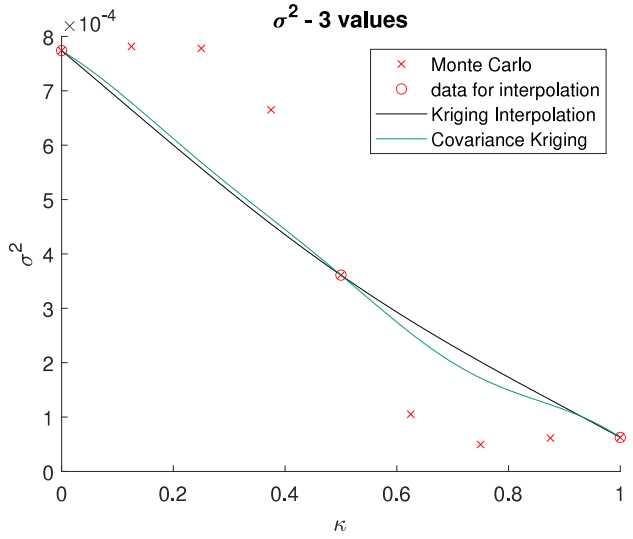

Fig. 21. Variance of λ with experiment data and interpolation with Kriging and Covariance Kriging using 3 load cases.

cases to 33 %, respectively. Of course,Monte Carlo simulations can be parallelized easily, however the computational cost still remains the same even if the time is reduced.

4. Conclusion

This analysis shows, that the sensitivity of geometric imperfections of cylindrical shells under pure torsion is not as strong compared to pure axial compression. This is expressed in a reduced standard deviation and a lower mean value of the results of the MCA compared to the load case with pure axial compression. Design guidelines address this by using different knockdown factors for different loadings. However, assuming a linear interaction for different ratios of each load, is not sufficient as shown. The presented method accurately interpolates the load cases. Furthermore, the stochastic moments of arbitrary unknown load combinations can be interpolated with this approach to account for them in the design process. A weakness of this approach is the high number of load cases which have to be taken into account to have a solid base for the interpolation method since a higher number of load

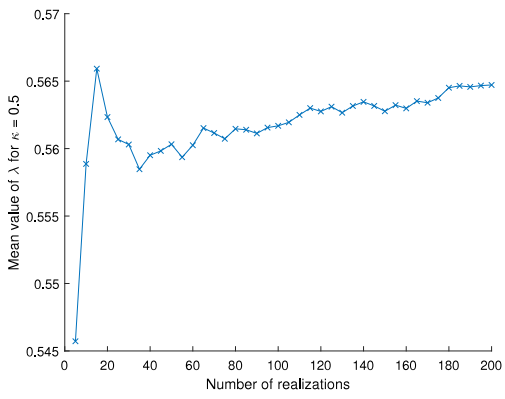

Fig. 22. Convergence Plot of the mean value for $\kappa = 0.5$ of the Monte Carlo Simulation.

cases for the interpolation result in a better interpolation. A topic for future works should be the experimental probabilistic investigation for the combined load case of axial compression and torsion.

CRediT authorship contribution statement

Niklas Reuter: Writing – review & editing, Writing – original draft, Visualization, Methodology, Investigation. **Benedikt Kriegesmann:** Writing – review & editing, Writing – original draft, Supervision, Project administration, Methodology, Funding acquisition, Conceptualization.

Declaration of competing interest

The authors declare that they have no known competing financial interests or personal relationships that could have appeared to influence the work reported in this paper.

Acknowledgments

This research was founded by the German Research Foundation (Deutsche Forschungsgemeinschaft, DFG) via project No. 463883313. The statements in this contribution do not necessarily represent the opinion of the DFG.

Appendix

See Fig. 22.

Data availability

No data was used for the research described in the article.

References

[1] M.W. Hilburger, Buckling of Thin-Walled Circular Cylinders, NASA, 2020, NASA SP-8007/REV2.
[2] J. Singer, T. Weller, J. Arbocz, Buckling Experiments: Experimental Methods in Buckling of Thin-Walled Structures, 1, Wiley, New York, 1997.
[3] J. Singer, T. Weller, J. Arbocz, Buckling Experiments: Experimental Methods in Buckling of Thin-Walled Structures, vol. 2, John Wiley & Sons, Inc., Hoboken, NJ, USA, 2002.
[4] J. Arbocz, Past, present and future of shell stability analysis, Z. Für Flugwiss. Und Weltraumforsch. 5 (6) (1981) 335–348.
[5] I. Elishakoff, Uncertain buckling: Its past, present and future, Int. J. Solids Struct. 37 (46–47) (2000) 6869–6889, http://dx.doi.org/10.1016/S0020-7683(99)00318-2.
[6] T.A. Winterstetter, H. Schmidt, Stability of circular cylindrical steel shells under combined loading, Thin-Walled Struct. 40 (10) (2002) 893–910, http://dx.doi.org/10.1016/S0263-8231(02)00006-X.

[7] General Rules: Strength and Stability of Shell Structures, Brussels, Belgium, 2002, Eurocode 3 Part 1.6.
[8] N. Reuter, S. Panek, B. Kriegesmann, G. Balokas, T.S. Hartwich, D. Krause, Experimental investigation and probabilistic analysis of the buckling load of isotropic cylinders under multiaxial loading, Thin-Walled Struct. 205 (2024) 112379, http://dx.doi.org/10.1016/j.tws.2024.112379, URL https://www.sciencedirect.com/science/article/pii/S0263823124008206.
[9] V.V. Bolotin, Statistical aspects in the theory of structural stability, in: G. Herrmann (Ed.), Dynamic Stability of Structures, Pergamon Press, 1967, pp. 67–81.
[10] A. Haldar, S. Mahadevan, Probability, Reliability and Statistical Methods in Engineering Design, first ed., John Wiley & Sons, 1999.
[11] I. Elishakoff, Probabilistic Theory of Structures, Dover, 1999.
[12] J. Arbocz, H. Abramovich, The Initial Imperfection Data Bank at the Delft University of Technology: Part I, Tech. Rep. LR-290, TU Delft, LR-290, 1979.
[13] I. Elishakoff, J. Arbocz, Reliability of axially compressed cylindrical shells with general nonsymmetric imperfections, Trans. the ASME 52 (1985) 122–128.
[14] I. Elishakoff, S. van Manen, P.G. Vermeulen, J. Arbocz, First-order second-moment analysis of the buckling of shells with random imperfections, AIAA J. 25 (8) (1987) 1113–1117.
[15] M.K. Chryssanthopoulos, M.J. Baker, P.J. Dowing, Imperfection modeling for buckling analysis of stiffened cylinders, J. Struct. Eng. 117 (7) (1991) 1998–2017.
[16] J. Arbocz, M.W. Hilburger, Toward a probabilistic preliminary design criterion for buckling critical composite shells, AIAA J. 43 (8) (2005) 1823–1827.
[17] M. Biagi, F. Del Medico, Reliability-based knockdown factors for composite cylindrical shells under axial compression, Thin-Walled Struct. 46 (12) (2008) 1351–1358.
[18] C.C. Chamis, G.H. Abumeri, Probabilistic dynamic buckling of composite shell structures, Compos. Part A: Appl. Sci. Manuf. 36 (10) (2005) 1368–1380, http://dx.doi.org/10.1016/j.compositesa.2004.11.018.
[19] R. Degenhardt, A. Kling, A. Bethge, J. Orf, L. Kärger, R. Zimmermann, K. Rohwer, A. Calvi, Investigations on imperfection sensitivity and deduction of improved knock-down factors for unstiffened CFRP cylindrical shells, Compos. Struct. 92 (8) (2010) 1939–1946.
[20] M. Broggi, A. Calvi, G.I. Schuëller, Reliability assessment of axially compressed composite cylindrical shells with random imperfections, Int. J. Struct. Stab. Dyn. 11 (2) (2011) 215, http://dx.doi.org/10.1142/S0219455411004063.
[21] B. Kriegesmann, R. Rolfes, C. Hühne, A. Kling, Fast probabilistic design procedure for axially compressed composite cylinders, Compos. Struct. 93 (2011) 3140–3149, http://dx.doi.org/10.1016/j.compstruct.2011.06.017.
[22] M.W. Hilburger, Buckling of Thin-Walled Circular Cylinders, Tech. Rep., NASA SP-8007, 2020.
[23] P. Wriggers, Nonlinear Finite Element Method, Springer Berlin Heidelberg, 2008, http://dx.doi.org/10.1007/978-3-540-71001-1_1, URL http://link.springer.com/chapter/10.1007/978-3-540-71001-1_1.
[24] W.C.M.v. Beers, J.P.C. Kleijnen, Kriging for interpolation in random simulation, J. Oper. Res. Soc. 54 (3) (2003) 255–262, Publisher: Palgrave Macmillan Journals, URL https://www.jstor.org/stable/4101619.
[25] Z. Wang, J.H.S. Almeida Jr., L. St-Pierre, Z. Wang, S.G.P. Castro, Reliability-based buckling optimization with an accelerated kriging metamodel for filament-wound variable angle tow composite cylinders, Compos. Struct. 254 (2020) 112821, http://dx.doi.org/10.1016/j.compstruct.2020.112821, URL https://www.sciencedirect.com/science/article/pii/S0263822320327471.
[26] C. Hühne, R. Rolfes, E. Breitbach, J. Teßmer, Robust design of composite cylindrical shells under axial compression – simulation and validation, Thin-Walled Struct. 46 (7–9) (2008) 947–962, http://dx.doi.org/10.1016/j.tws.2008.01.043.
[27] B. Kriegesmann, R. Rolfes, C. Hühne, J. Teßmer, J. Arbocz, Probabilistic design of axially compressed composite cylinders with geometric and loading imperfections, Int. J. Struct. Stab. Dyn. 10 (4) (2010) 623–644, http://dx.doi.org/10.1142/S0219455410003658.